Physical limits to spatial resolution of optical recording: Clarifying the spatial structure of cortical hypercolumns

Jonathan R. Polimeni*, Domhnull Granquist-Fraser†, Richard J. Wood†, and Eric L. Schwartz*†‡§

Departments of *Electrical and Computer Engineering and †Cognitive and Neural Systems, Boston University, Boston, MA 02215; and ‡Department of Anatomy and Neurobiology, Boston University Medical School, Boston, MA 02118

Communicated by David H. Hubel, Harvard Medical School, Boston, MA, January 21, 2005 (received for review December 3, 2004)

Neurons in macaque primary visual cortex are spatially arranged by their global topographic position and in at least three overlapping local modular systems: ocular dominance columns, orientation pinwheels, and cytochrome oxidase (CO) blobs. Individual neurons in the blobs are not tuned to orientation, and populations of neurons in the pinwheel center regions show weak orientation tuning, suggesting a close relation between pinwheel centers and CO blobs. However, this hypothesis has been challenged by a series of optical recording experiments. In this report, we show that the statistical error associated with photon scatter and absorption in brain tissue combined with the blurring introduced by the optics of the imaging system has typically been in the range of 250 μm. These physical limitations cause a systematic error in the location of pinwheel centers because of the vectorial nature of these patterns, such that the apparent location of a pinwheel center measured by optical recording is never (on average) in the correct *in vivo* location. The systematic positional offset is $\approx$116 μm, which is large enough to account for the claimed misalignment of CO blobs and pinwheel centers. Thus, optical recording, as it has been used to date, has insufficient spatial resolution to accurately locate pinwheel centers. The earlier hypothesis that CO blobs and pinwheel centers are coterminous remains the only hypothesis currently supported by reliable observation.

hypercolumn model | orientation maps | visual cortex | cytochrome oxidase blobs

The columnar organization of the neocortex is one of the seminal discoveries in neurobiology (1, 2). Neurons in vertical register within the cortex tend to have similar response properties, such as selectivity for oriented visual stimuli and ocular dominance (2). Perhaps even more important, however, was the discovery that columns were themselves organized into larger structures, termed hypercolumns, comprised of the full 180° range of orientation tuning for both eyes on the scale of $\approx$1 mm (3, 4). This idea has proven vital because it suggested a basic uniformity of cortical structure and a principle around which it might be organized. Because hypercolumn structure is critical to theories of both cortical function and its development, clarifying its details has been a central goal of neuroscience.

Horton and Hubel (5, 6) showed that an additional periodic anatomical feature of primate visual cortex, the cytochrome oxidase (CO) blob system, consists of patches of cortical tissue most prominently appearing in layers II/III but also appearing in layers I, IVb, V, and VI, with a size of $\approx 150 \times 250$ μm in primary visual cortex (V1) of macaque, and exhibiting higher-than-average metabolic activity, hence, staining darkly for CO activity. They observed the CO blob density to be approximately five per mm^2, although Horton and Hocking (7) showed variation of a factor of two across subjects. The receptive field properties of neurons in the blobs is still an area of active research, but Livingstone and Hubel (8) demonstrated that unoriented, chromatically tuned receptive fields are a characteristic feature of neurons located within the blobs. Through careful alignment of anatomical data, Horton and Hubel (5, 6) found that CO blobs generally lie at the centers of ocular dominance columns and have an average period, in macaque, of $\approx$350 μm in the direction parallel to local ocular dominance column boundaries, and 550 μm perpendicular, demonstrating an interrelationship between these two anatomical systems that inspired the incorporation of the blob system into a revised hypercolumn model (6, 8).

The pinwheel pattern (9) of orientation tuning columns in visual cortex, first observed with optical recording (10, 11), is arguably the single most widely recognized icon of cortical functional architecture. This pattern represents the spatial layout of neurons in visual cortex responsive to oriented visual stimuli, characterized by orientation singularities at the pinwheel centers (where locally the map exhibits tuning to the full 180° of orientations) surrounded by regions where orientation preference changes smoothly.

Optical recording studies have shown that pinwheel centers, like the CO blobs, are aligned with ocular dominance column centers in macaque V1 (10, 12). The neurons within the CO blob regions are not tuned to orientation, and the centers of cortical pinwheels, at least at the level of population response, are also weakly tuned to orientation. The hypothesis that CO blobs and pinwheel centers are coterminous was thought to establish the basic structure of the cortical hypercolumn. [This hypercolumn model had been suggested previously by Horton (ref. 6, figure 49) and by Blasdel and Grinvald (ref. 13, figure 14).]

However, this parsimonious version of the hypercolumn is inconsistent with three experimental reports. Bartfeld and Grinvald (14) reported evidence, based on joint *in vivo* optical recording of intrinsic signals and CO histology in macaque V1, that CO blobs and orientation pinwheels are not aligned. In apparent support of this observation, they also reported that orientation tuning of neurons near the putative pinwheel centers was no different from those in more distal locations. However, no spatial error analysis was presented in this work.

The latter of these two observations of Bartfeld and Grinvald (14) was followed up, in greater detail, by Maldonado *et al.* (15). They used a combination of tetrode electrophysiology and optical recording of intrinsic signals in cat areas 17 and 18 to claim that orientation tuning in the pinwheel centers is as strong as in the surrounding area. Maldonado *et al.* (15) supported their claim by pointing out that the optical recording signal is a population average, and so individual neurons in the pinwheel centers, even if they were strongly tuned to orientation, would average to a weak population response at the pinwheel centers imaged through optical recording. However, these authors also did not discuss potential consequences of spatial blur in optical

Abbreviations: V1, primary visual cortex; CO, cytochrome oxidase; FWHM, full width at half maximum; PSF, point-spread function; SNR, signal-to-noise ratio.

§To whom correspondence should be addressed. E-mail: eric@bu.edu.

www.pnas.org/cgi/doi/10.1073/pnas.0500291102

recording, nor did they provide any detailed error analysis of their observations. Although the experiment of Bartfeld and Grinvald (14) was in primates, and that of Maldonado *et al.* (15) was in cats, these two results are widely seen to make the seemingly consistent argument that orientation tuning at pinwheel centers is strong. Because CO blobs exhibit little or no orientation tuning, this purported strong orientation tuning at the pinwheel centers is consistent with the hypothesis that pinwheel centers do not coincide with the CO blobs.

In support of the observations of Grinvald and colleagues, a recent joint *in vivo* optical recording of intrinsic signals and CO histology experiment performed in owl monkey V1 by Xu *et al.* (16) estimated that pinwheel density is roughly twice that of CO blob density. If the densities of these two systems were to differ markedly, the systems could not be in one-to-one alignment.

Grinvald and colleagues (14, 17) have rejected the previously established classical model that pinwheel centers and CO blobs are aligned. In its place, they suggested an alternate hypercolumn model, based on their optical recording observations, that depicts the pinwheel centers and the CO blobs staggered and out of alignment. This hypothesis has been widely accepted and now appears in textbooks (see, e.g., ref. 18). In this report, we show that a careful quantification of the physical limits to the spatial resolution of optical recording based on an analysis of photon scatter and macroscope optics, combined with an understanding of the mathematical properties of orientation maps, demonstrates that there is insufficient spatial resolution in optical recording, as it has generally been used to date, to reject the classical model.

Establishing the precise alignment of submillimeter modular systems in the brain requires a careful error analysis because systematic errors in the range of even 100 μm could lead to false displacement of two different modular systems. One source of error is the unavoidable fact that any optical system has finite spatial resolution and thus introduces non-zero spatial blur. The point-spread function (PSF), characterized by its full width at half maximum (FWHM), is a common measure of the spatial resolution of an optical system. The physical lower limit for the PSF of optical recording is provided by the joint effects of photon scatter in the turbid cortical tissue and the depth of field of the optical system.

It is so important to clarify the details of spatial resolution and identify sources of spatial filtering because of the vectorial nature of cortical orientation maps. Blur (i.e., spatial averaging) is usually considered in terms of a scalar-valued image source, e.g., a conventional photograph. However, cortical orientation maps that encode both magnitude and orientation at each pixel are vector-valued images. The peaks in a scalar-valued image, such as a photograph, will have negligible positional error associated with isotropic Gaussian blur: the center of a blurred spot will be, on average, in the correct position. However, a vector-valued image, such as a cortical orientation map, has a systematic positional error associated with spatial blur.

The easiest way to understand the difference between blurring scalar- and vector-valued data is to note what happens when one attempts to arithmetically average orientations. (Recall that orientation is defined between 0° and 180°.) The average of the numbers 0 and 180 is 90. However, the average of the orientations 0° and 180° is not 90°, but, rather, it is 0° (or 180°). This phenomenon is often called phase wrapping in one-dimensional signal processing. Orientations do not obey the same rules of arithmetic as do numbers. As a consequence, blur induces non-zero mean error for singularity location in vector-valued images (19, 20, ¶). (A computer animation illustrating the behavior of orientation maps due to various amounts of spatial blur, which is discussed in detail below, can be seen in Movie 1 and Fig. 4, which are published as supporting information on the PNAS web site.)

Additional information can be found in Figs. 5–11, which are published as supporting information on the PNAS web site.

To date, the only detailed experimental measurement of the resolution of optical recording (that we are aware of) was provided by Orbach and Cohen (21), who report a PSF of 200 μm FWHM calculated based on imaging a pinhole in aluminum foil through 500 μm of resected salamander olfactory bulb.

Contradicting this experimental result, several authoritative reviews of optical recording report estimates that are much smaller than the measurement of Orbach and Cohen (21). For example, one review states that the resolution of optical recordings is in the range of 50–100 μm (22). Another review states that it is better than 50 μm (17). These claims were not supported by any accompanying computational or experimental evidence.‖ Moreover, these same reviews state that one advantage of the narrow depth of field of the macroscope is that the vasculature on the cortical surface is removed by defocus: the depth of field is so narrow that relatively large blood vessels are blurred enough that they vanish. Because columnar structure in the brain is extensive in depth (so that the entire vertical extent of a cortical column can never be simultaneously in focus), the neuronal response and surface vessels will also experience significant blur. One of the chief goals of the present work is to analyze this optical blur and unavoidable photon scatter in detail.

In this report, we show that the statistical error associated with photon scatter and absorption in *in vivo* brain tissue combined with the optics of the imaging system, assuming standard experimental parameters, is in the range of 250 μm FWHM. Associated with the PSF is a systematic error in the location of pinwheel centers and a reduction in their density because of the vectorial nature of these patterns. Because this positional error is systematic rather than merely statistical, the apparent location of a pinwheel center measured by optical recording is never (on average) in the correct *in vivo* location. We estimate the magnitude of the mean systematic positional offset to be $\approx$116 μm for standard experimental parameters. This offset is large enough to account for the claimed misalignment of the two columnar systems. Because the application of spatial filters in postprocessing is typical in optical recording data analysis (e.g., ref. 16), we also illustrate the effects of band-pass postprocess filtering, which are as problematic as the low-pass filtering associated with the physical lower limit for resolution. The error induced by postprocessing depends on the signal-to-noise ratio (SNR) and the parameters of the spatial filters. We show, assuming a wide range of SNRs and commonly used filters, that postprocessing can inflate the pinwheel density by as much as 100% and can introduce substantial positional error in the location of orientation singularities.

¶Schwartz, E. L. & Rojer, A. S. (1992) *Soc. Neurosci. Abstr.* **18,** 742 (abstr.).

‖Grinvald and colleagues (14, 17) cite the PSF FWHM measured experimentally by Orbach and Cohen (21), but claim that the actual resolution of optical recording is two to four times higher than the reported value. They justify the higher resolution by stating that ''. . . if a differential map is calculated, the spatial resolution increases,'' (ref. 22, page 4177), and ''[the] reproducibility in location of the pinwheel centers suggests, that the resolution of differential optical recording may be better than 50 μm'' (ref. 17, page 34). No evidence or detailed discussion is presented to corroborate the claim that differential imaging can reduce the point spread measured by Orbach and Cohen (21) by 400%. It is certainly true that differential imaging improves the SNR of optical recording because it will reject common-mode noise signals. However, improving the basic PSF of an optical system, i.e., the spatial resolution, requires deconvolution techniques, sometimes called super-resolution (23, 24). Successful deconvolution requires very high SNR and very good understanding of both the signal and the noise. Neither of these conditions holds for optical recording. Additionally, reproducibility of a measurement is necessary for precision, but is insufficient to guarantee accuracy. An inaccurate measurement, associated with a systematic error, is exactly reproducible. Therefore, the reproducibility over time of optical recording says nothing about the underlying spatial resolution.

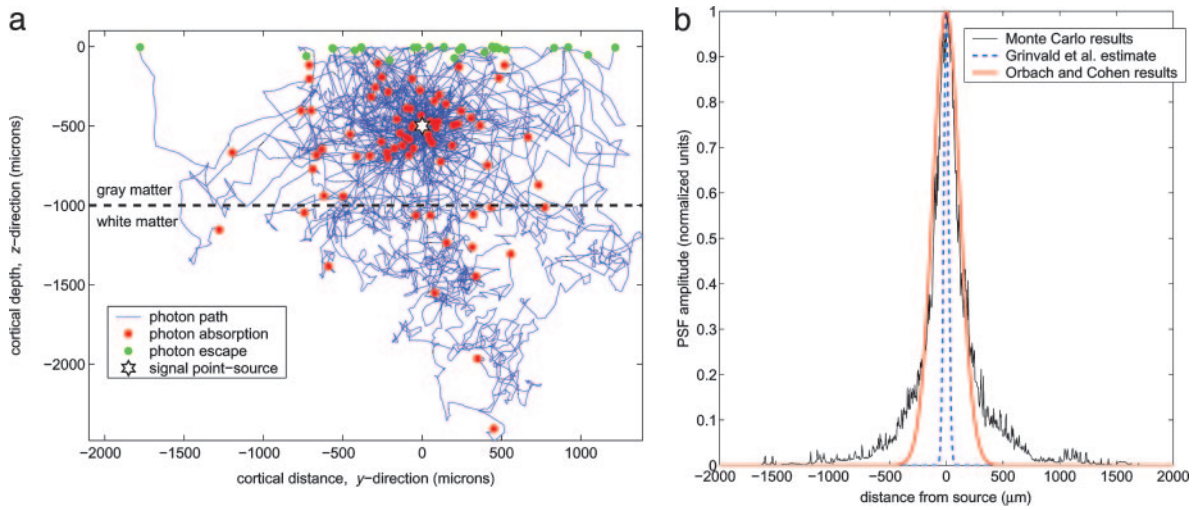

Fig. 1. Monte Carlo simulation. (*a*) Sample of 100 model photon paths in cortical tissue. Cortical gray matter, in this example, was taken to be 1,000 μm thick, and the gray matter/white matter interface is denoted by a dashed black line. The white star marks the model photon source 500 μm below the gray matter/air interface. Red dots mark points at which a photon was absorbed. Green dots mark points at which photons exit the tissue. The small 1-mm thickness of gray matter illustrated here demonstrates the qualitative difference as the model photon travels through gray matter versus white matter. However, in our simulations, cortical gray matter of 2.3-mm thickness was used, and each PSF was computed from 10^6 photons per reflectance source. (*b*) Resultant columnar PSF, averaged over sources at 200–500 μm cortical depth, with macroscope focus set at a depth of 300 μm. The FWHM is 234.3 μm. Also shown are a 280-μm FWHM Gaussian function, which is the result of Orbach and Cohen (21) (corrected by our Monte Carlo results for missing back-scatter), and a 50-μm FWHM Gaussian function, which is suggested as a possible value by Grinvald *et al.* (17).

Materials and Methods

To determine the physical limits on spatial resolution of optical recording, we used standard Monte Carlo methods (25) to model photon scatter and absorption in gray matter and white matter for photons of wavelength 633 nm (a commonly used optical recording light source) together with a diffractive optics modeling system to study the depth of field of the macroscope (26) (a lens system commonly used for image acquisition in optical recording).** Our goal was to provide the limiting physical PSF in cortical tissue due to photon scatter and optics. We did not address the additional biological aspects of this problem, which can only make the PSF broader.†† Therefore, our results provide a conservative physical limit on the best possible spatial resolution obtainable with this technique.

An example of our simulation results for the scattering of 633-nm wavelength photons by a reflectance point source in cortical tissue is illustrated in Fig. 1. Because of the turbid nature of cortex, the trajectories of photons reflected by a point source exhibit a three-dimensional "fuzz-ball" structure depicted in Fig. 1*a*. Note that photons which ultimately escape cortex, those photons that comprise the image, predominantly exit from shallow tissue depths.

To compute the photon-scatter PSF, we calculated, for each location in the three-dimensional model cortex, the probability of a photon scattering to that location from a fixed reflectance point. We also obtained the optical transfer function of the macroscope by using an industry standard diffractive optics modeling system (see *Supporting Text*, which is published as supporting information on the PNAS web site, and Figs. 7 and 8). We then combined through convolution the photon-scatter distribution with the macroscope transfer function, and averaged over cortical depths from 200 to 500 μm to obtain a columnar PSF to emulate the response to a signal source emanating from a column of activated neurons. The columnar PSF for a model experiment with a focal depth of 300 μm is presented in Fig. 1*b*, demonstrating a resulting FWHM of $\approx$240 μm. [Note that the FWHM of the PSF is a function of focal depth; it significantly broadens as the focal point is positioned deeper into cortical tissue (28). This finding suggests that minimization of optical blur is achieved by focusing near the cortical surface (see, e.g., ref. 29) rather than focusing at 300–600 μm below the cortical surface, as is common.] For reference, in the same plot, we show a 50-μm FWHM Gaussian PSF, as reported by Grinvald *et al.* (17), and a 280-μm FWHM Gaussian PSF, corresponding to the *in vitro* observations of Orbach and Cohen (21) adjusted to *in vivo* conditions (see *Supporting Text*), and the 240-μm FWHM PSF that was determined from our Monte Carlo simulation of the photon-scatter and macroscope-optics model. The heavy tails of the resultant columnar PSF suggest that the function is better modeled as a Cauchy function than as a Gaussian function; see *Supporting Text* for a discussion comparing these two functions.

The results of our detailed Monte Carlo simulation and diffractive optics model and the adjusted experimental measurement of Orbach and Cohen (21) demonstrate that the spatial resolution of optical recording is far lower than the typical estimates. What are the consequences of this lower resolution for the interpretation of the data? We used computational modeling to evaluate the effect of the spatial blur inherent to optical recording on the observed pinwheel pattern.

A simulated pinwheel pattern (see Fig. 9 for details) of periodicity matching the CO blob system (i.e., 350 $\times$ 550 μm) was created by using band-pass-filtered random orientation values (30) and is shown in Fig. 2*a*. The result of blurring this map with a Cauchy low-pass filter of 240-μm FWHM is shown in Fig. 2*b*. (Note that blurring the pinwheel pattern is identical to blurring the individual orientation response images that are used to form the pinwheel pattern; see *Supporting Text* and Figs. 10 and 11.) Although the original and blurred pinwheel maps are qualitatively similar in appearance, they are quantitatively very

Granquist-Fraser, D., Polimeni, J. & Schwartz, E. L. (2003) *Soc. Neurosci. Abstr.* **29, 125.3 (abstr.).

††"Microlensing" caused by dense layers of cell bodies has been mentioned as a serious source of optical recording interference (27). Biological sources of spatial blur include hemodynamics, heart pulsation, and the generally poorly understood nature of the coupling of neural activation to changes in the optical properties of tissue, and the underlying noise and spontaneous neural activity.

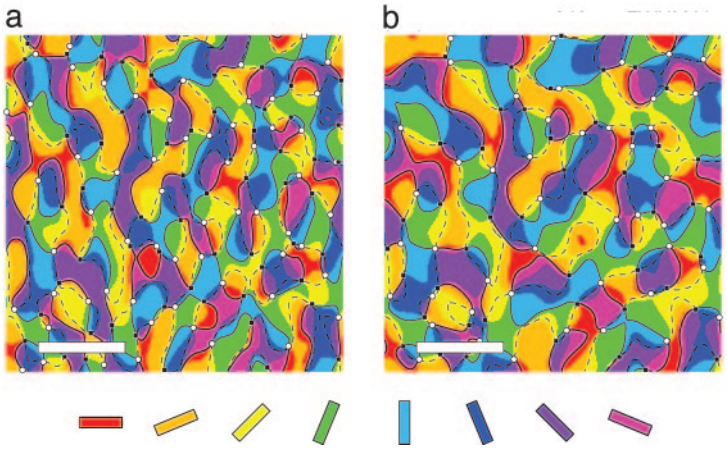

Fig. 2. Results of blurring orientation data. (*a*) Synthetic orientation tuning data generated by band-pass filtering random orientation values (30). The original average distance between pinwheel centers is set at 350 × 550 μm, and the number of pinwheels is 124. Positive chirality (i.e., right-handed) pinwheels are indicated by white circles and negative chirality is indicated by black squares. The solid and dashed black lines trace out zero-crossings of the orientation map, whose intersections mark the pinwheel center locations for a continuous orientation map, a result known as the sign theorem (36). (*b*) Blurring the data of *a* with a Cauchy filter whose FWHM is 240 μm results in an average pinwheel distance of 499.1 μm and 93 pinwheels. If the pattern in *a* is taken as the true *in vivo* orientation map, the pattern in *b* is that one that would be produced by imaging with the blur that we have estimated from our joint photon-scatter simulations and optics model. The pseudocolor map of orientation is provided below. (Scale bars, 1 mm.)

different. (Note also that we have conservatively assumed that there is no spatial noise and no postprocess filtering; relaxing these assumptions leads to much greater errors, as shown below.)

Results

Our computer simulation results establish three important effects of spatial filtering on the orientation map spatial structure:

1. Orientation singularities approach and annihilate in left- and right-handed pairs when increasing amounts of spatial blur are applied. Therefore, the measured density of pinwheels is significantly reduced and the measured spacing is significantly increased by the blur inherent in optical recording (see *Supporting Text*).
2. Orientation singularity position is systematically offset as a function of spatial blur. The observed pinwheel position is, on average, displaced from the correct *in vivo* position by a mean of 116 μm.
3. Orientation responses far from singularities are more spatially stable under blur than that near pinwheel centers.

The systematic error associated with low-pass filtering orientation maps was studied by varying the presumed blur over a large range and generating 1,000 simulated orientation maps for each FWHM. The results are summarized in Fig. 3*a*. For a simulated *in vivo* pinwheel pattern with 350 × 550 μm periodicity and a Cauchy-distributed spatial blur with FWHM of 240 μm, both the density and the total number of pinwheels is reduced

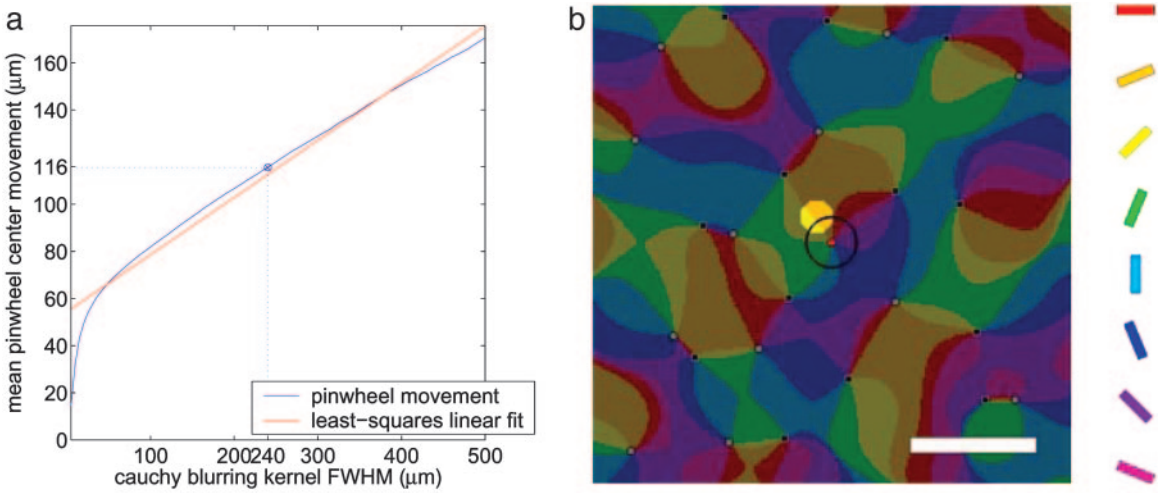

Fig. 3. Effects of blur on pinwheel center position. (*a*) Simulation of pinwheel movement and annihilation due to low-pass filtering with increasing FWHM to 1,000 *in vivo* pinwheel patterns with 350 × 550-μm spacing. As the Cauchy blurring kernel broadens, the average pinwheel movement increases nearly linearly, resulting in a bias in the observed singularity location relative to the true *in vivo* location of the singularity. At 240 μm FWHM, the orientation singularity position error is 116 μm on average. (*b*) Simulation of the experiment of Maldonado *et al.* (15). The offset of the tetrode recording site from the true orientation singularity location is demonstrated on a synthetic orientation tuning preference map. Here, the tetrode is illustrated by a spotlight of radius 65 μm offset from a orientation singularity by 116 μm. In this example, the tetrode observes an orientation range of ≈40°. The black ring marks the area of a CO blob with a 100-μm radius centered at the chosen orientation singularity, and the areas of the tetrode recording and the CO blob exhibit little overlap. (Scale bar, 500 μm.)

through annihilation of neighboring right- and left-handed pinwheels by ≈25%, and a systematic bias in their position of 116 μm is introduced. The results for the full range of blurs are shown in Fig. 3*a* and are illustrated in Movie 1.

Our results indicate that (*i*) pinwheel density, in the absence of spatial noise and postprocessing, is underestimated by an amount determined by the magnitude of blur in the imaging technique and the veridical *in vivo* spacing; and (*ii*) the observed position of pinwheel centers is systematically offset from the true position by the imaging blur. This result is a bias, a non-zero mean error, in the blurred data. This finding means that the optically imaged position of a cortical pinwheel is never correct, but that it is offset from the true *in vivo* location.

These results require a reinterpretation of the observations of Bartfeld and Grinvald (14) and of Maldonado *et al.* (15). In the case of the Bartfeld and Grinvald (14) experiment, the pinwheel patterns generated by their optical recording are blurred versions of the true cortical pinwheel patterns and are therefore subject to the same pinwheel center offset that we see in simulation. Therefore, one can expect an average displacement of the observed pinwheel centers from their true locations on the order of 116 μm, which is enough to shift the pinwheel centers outside of the blob regions if the pinwheel centers and the CO blobs were truly aligned as in the classical model. Based on this argument, the results of the Bartfeld and Grinvald (14) experiment are insufficient to disprove that the two systems are aligned.

A further illustration of the scale of CO blobs in the macaque *vis-à-vis* the systematic error in pinwheel location is shown in Fig. 3*b*. Here, a synthetic pinwheel pattern, computed based on typical macaque parameters, is displayed with a 100-μm radius circular ring representing a CO blob centered on a pinwheel center. The spotlight superimposed on the pinwheel pattern above the CO blob region represents the reported 65-μm radius recording area of the tetrode [as used in the cat by Maldonado *et al.* (15)] displaced 116 μm away from the pinwheel center. This illustration demonstrates that the 116-μm pinwheel center displacement predicted by our simulations is sufficient to shift their tetrode placement enough for the tetrode recording area and the actual CO blob region to exhibit little overlap.

Pinwheel center offsets of this magnitude may also account for the observed range of orientations near pinwheel centers reported by Maldonado *et al.* (15) in the cat. The expected result for a tetrode placed at a pinwheel center would be to observe nearly a full 180° range of tuning in the neighborhood of the tetrode. We find that a 240-μm blur yields an average pinwheel offset of ≈116 μm, and this would correspond, within a tetrode recording radius, to an average observed orientation range of 43.2° (based on macaque pinwheel spacing parameters), which is very similar to the range reported by Maldonado *et al.* (15) of 39.2° at the (purported) pinwheel centers. Had their tetrode been placed at an actual pinwheel center, an orientation range of 180° would be expected. This analysis supports our hypothesis that their tetrode was systematically located in a region of the cortex significantly distant, perhaps up to 100 μm, from the actual *in vivo* pinwheel center. (The results of our tetrode experiment simulation are presented in Fig. 5.) It is likely that the optical recording data systematically misguided their tetrode placement such that observations of cells exhibiting strong orientation tuning were made from cells that were not in fact located in the true pinwheel centers.

The results presented thus far have only assumed sources of spatial blur attributable to purely physical phenomena, namely, photon scatter in tissue and optical point spread. These results, therefore, ultimately speak to the physical limitations of optical recording and the effects of its resolution on the analysis of orientation maps. It is common practice, however, to intentionally introduce spatial filtering during data postprocessing to eliminate unwanted spatial noise. This filtering can affect the position and density of orientation singularities and thus can impact observations on the alignment of the pinwheel pattern and CO blob system.

In Fig. 6, we briefly present the consequences of applying band-pass postprocess filters used in the recent Xu *et al.* (16) study that reported a higher density of orientation singularities than CO blobs. Our simulation shows that even assuming unrealistically high SNRs (in the range of 10–100), applying the same band-pass postprocess filters used by Xu *et al.* (16) introduces artifactual pinwheels, nearly doubling the initial density, and induces substantial positional error for the orientation singularities. As demonstrated by the results shown in Fig. 6, this effect is strongly dependent on the spatial SNR of the data, with smaller SNR increasing the error. Thus, even though Xu *et al.* (16) took steps, following the recommendations in a preliminary version of this report**, to minimize physical blur by focusing shallowly in the cortical tissue during optical recording, their use of postprocess filters undermines their conclusion that the pinwheel and CO blob systems are misaligned.

Discussion

Optical recording, when used to image scalar-valued distributions such as the intensity patterns measured in visual topography experiments (31), is much less sensitive to resolution limits than vector-valued images because scalar-valued images are expected to have an ≈0 mean error associated with blur. Additionally, a significant component of the spatial blur analyzed here is caused by the macroscope because of its very narrow depth of field (26). Although the large light-gathering properties of this instrument are an advantage for many applications, it is perhaps not the best choice of optics for sensitive spatial measurement of vector-valued patterns. Furthermore, the common practice of focusing at depths significantly below the very top layer of cortex, where photons escape into the instrument, is a significant cause of error.

Scalar-valued imaging was used in several optical recording experiments (32, 33) to locate CO blobs *in vivo*. This approach is expected to be free of the systematic location error associated with using the pinwheel formalism. By using the blob imagery as a guide, it should be possible to make extensive electrode penetrations in a small number of blob regions and the corresponding extra-blob regions. If additional errors related to parallax and to alignment of *in vivo* and *in vitro* anatomical patterns were carefully handled, the details of blob and extra-blob hypercolumn structure could be further clarified by this approach.

Voltage-sensitive dye imaging (34) has the same physical limits on resolution from photon scatter and optics as does intrinsic optical recording. However, limiting the vertical range of dye penetration to superficial cortex could provide the benefit of limiting the extension in depth of the optical source. Then, appropriate focus of the optical system would provide a considerably more favorable columnar PSF. An emerging high-resolution imaging technique that uses laser-scanning fluorescence microscopy with multiphoton excitation avoids the problems of photon scatter because all photons collected from a particular scan position emanate from a single excitation point in the tissue (27, ‡‡).

Optical recording is a major addition to the tools available for exploring functional neuroanatomy. However, until recently, there has been little appreciation of the dependence of results obtained with optical recording, particularly the imaging of

‡‡Ohki, K., Kara, P. & Reid, R. C. (2004) *Soc. Neurosci. Abstr.* **30,** 646.2 (abstr.).

vector-valued orientation maps in visual cortex on spatial resolution. The effective spatial filter that has been derived in this report, from Monte Carlo simulation and diffractive optics modeling, depends in a complicated way on the wavelength of light, the depth of field of the optics, the choice of focal depth, and the extent of vertical summation. By illuminating with light at 633-nm wavelength, imaging through macroscope optics, and assuming a columnar structure that extends from 200 to 500 μm, we have found that the effective FWHM of the physical component of blur is $\approx$250 μm at a focal depth of 300 μm. This finding argues that optical recording resolution is much coarser than is commonly assumed, which leads to serious errors in the estimation of the quantitative properties of orientation maps. Postprocess spatial filtering, which is widely used, can cause large additional variations in observed pinwheel center density and position.

Our results are comparable to those provided by Orbach and Cohen (21), and with the recent Monte Carlo study of Deng and Gu (35), who found a PSF FWHM of $\approx$350 μm for 400-nm wavelength light at a focal depth of 500 μm with a 0.25 numerical aperture lens. We emphasize that the experiment of Orbach and Cohen (21) and the simulation of Deng and Gu (35) refer to slightly different conditions from those that we studied, which are specific to the macroscope and to columnar neuronal structure. Nevertheless, all three results suggest a spatial resolution in the range of 300-μm FWHM.

Error analysis in this area has been neglected and must become a standard requirement for quantitative study of hypercolumn structure. In this context, it would be extremely desirable to directly measure the columnar PSF, for example, by imaging fluorescent beads embedded in tissue at different cortical depths. Then, the analysis and simulation methods outlined here could be used as a guide to establish error bounds for individual experiments for the specific optics, wavelength, and depth of focus used.

The conclusion of our analysis is that optical recording, as it has been used to date, does not have sufficient accuracy to determine the spatial relationship between the CO blob and the orientation pinwheel systems. Hopefully, techniques such as multiphoton optical recording will succeed in resolving this issue that is central to understanding the functional architecture of visual cortex. At the present time, at least one detailed microelectrode study (8) has affirmed what we term the classical model for the cortical hypercolumn: cells in CO blobs exhibiting poor orientation tuning lie at the centers of orientation pinwheels, and CO blobs and pinwheel centers spatially coincide. Subsequent rejections of it, through optical recording methods, are clouded by methodological problems and do not stand up to the conservative error analysis provided in this article.

We thank Gary Blasdel (Northwestern University, Evanston, IL) for making us aware of the spatial blurring properties associated with the narrow depth of field achieved by the macroscope and for generously providing us with sample optical recording data. We also thank Rick Born, Jonathan Horton, David Hubel, Niall McLoughlin, Chris Pack, and Aaron Seitz for helpful discussions related to this work. All wave optics calculations were performed by using Breault Research Organization's Advanced Systems Analysis Program language. This software and training in its use was generously provided by Breault Research (Tucson, AZ). Alan Greynolds developed this software that includes macros for the Gaussian Beam decomposition methods used to model the macroscope optics. This work was supported by National Institutes of Health/National Institute of Biomedical Imaging and Bioengineering Grant EB001550.

1. Mountcastle, V. (1957) *J. Neurophysiol.* **20,** 408–434.
2. Hubel, D. & Wiesel, T. (1962) *J. Physiol. (London)* **160,** 106–154.
3. Hubel, D. & Wiesel, T. (1974) *J. Comp. Neurol.* **158,** 295–305.
4. Hubel, D. & Wiesel, T. (1977) *Proc. R. Soc. London Ser. B* **198,** 1–59.
5. Horton, J. & Hubel, D. (1981) *Nature* **292,** 762–764.
6. Horton, J. (1984) *Philos. Trans. R. Soc. London B* **304,** 255–272.
7. Horton, J. & Hocking, D. (1996) *J. Neurosci.* **16,** 7228–7239.
8. Livingstone, M. & Hubel, D. (1984) *J. Neurosci.* **4,** 309–356.
9. Braitenberg, V. & Braitenberg, C. (1979) *Biol. Cybern.* **33,** 179–186.
10. Blasdel, G. & Salama, G. (1986) *Nature* **321,** 579–585.
11. Grinvald, A., Lieke, E., Frostig, R., Gilbert, C. & Wiesel, T. (1986) *Nature* **324,** 361–364.
12. Blasdel, G. (1992) *J. Neurosci.* **12,** 3139–3161.
13. Blasdel, G. (1989) in *Sensory Processing in the Mammalian Brain*, ed. Lund, J. S. (Oxford Univ. Press, New York), Chapter 12, pp. 242–268.
14. Bartfeld, E. & Grinvald, A. (1992) *Proc. Natl. Acad. Sci. USA* **89,** 11905–11909.
15. Maldonado, P., Godecke, I., Gray, C. & Bonhoeffer, T. (1997) *Science* **276,** 1551–1555.
16. Xu, X., Bosking, W., Sary, G., Stefansic, J., Shima, D. & Casagrande, V. (2004) *J. Neurosci.* **24,** 6237–6247.
17. Grinvald, A., Shoham, D., Bonhoeffer, T., Ts'o, D., Frostig, A., Shmuel, A., Glaser, D., Vanzetta, I., Shtoyerman, E., Slovin, H., *et al.* (1999) in *Modern Techniques in Neuroscience Research*, eds. Windhorst, U. & Johansson, H. (Springer, New York), pp. 893–969.
18. Kandel, E., Schwartz, J. & Jessell, T., eds. (2000) in *Principles of Neural Science* (McGraw–Hill, New York), 4th. Ed, pp. 539–540.
19. Schwartz, E. & Rojer, A. (1994) In *Proceedings of the 12th IAPR International Conference on Pattern Recognition*, eds. Peleg, S. & Ullman, S. (IEEE Comput. Soc. Press, Los Alamitos, CA), Vol. 2, pp. 150–155.
20. Schwartz, E. (1994) in *Primary Visual Cortex in Primates*, eds. Peters, A. & Rockland, K. (Plenum, New York), Vol. 10, pp. 359–411.
21. Orbach, H. & Cohen, L. (1983) *J. Neurosci.* **3,** 2251–2262.
22. Bonhoeffer, T. & Grinvald, A. (1993) *J. Neurosci.* **13,** 4157–4180.
23. Baker, S. & Kanade, T. (2002) *IEEE Trans. Pattern Anal. Mach. Intell.* **24,** 1167–1183.
24. Elad, M. & Feuer, A. (1997) *IEEE Trans. Image Process.* **6,** 1646–1658.
25. Cheong, W.-F., Prahl, S. & Welch, A. (1990) *IEEE J. Quantum Electron.* **26,** 2166–2185.
26. Ratzlaff, E. & Grinvald, A. (1991) *J. Neurosci. Methods* **36,** 127–137.
27. Denk, W. & Svoboda, K. (1997) *Neuron* **18,** 351–357.
28. Granquist-Fraser, D. (2003) Ph.D. thesis (Boston Univ., Boston).
29. Schiessl, I. & McLoughlin, N. (2003) *NeuroImage* **20,** 1857–1864.
30. Rojer, A. & Schwartz, E. (1990) *Biol. Cybern.* **62,** 381–391.
31. Blasdel, G. & Campbell, D. (2001) *J. Neurosci.* **21,** 8286–8301.
32. Ts'o, D., Frostig, D., Lieke, E. & Grinvald, A. (1990) *Science* **249,** 417–420.
33. Vnek, N., Ramsden, B., Hung, C., Goldman-Rakic, P. & Roe, A. (1999) *Proc. Natl. Acad. Sci. USA* **96,** 4057–4060.
34. Grinvald, A. & Hildesheim, R. (2004) *Nat. Rev. Neurosci.* **5,** 874–885.
35. Deng, X. & Gu, M. (2003) *Appl. Opt.* **42,** 3321–3329.
36. Tal, D. & Schwartz, E. (1997) *Network Comput. Neural Syst.* **8,** 229–238.